Available online at www.sciencedirect.com
ScienceDirect
Journal of the Franklin Institute 344 (2007) 180–195
Journal of The Franklin Institute
www.elsevier.com/locate/jfranklin

Revealing the dynamic causal interdependence between neural and muscular signals in Parkinsonian tremor

S. Wang[a], Y. Chen[b], M. Ding[b], J. Feng[c], J.F. Stein[a], T.Z. Aziz[d], X. Liu[e,*]

[a]*University Laboratory of Physiology, University of Oxford, Parks Road, Oxford OX1 3PT, UK*
[b]*Department of Biomedical Engineering, University of Florida, USA*
[c]*Centre for Scientific Computing, University of Warwick, UK*
[d]*Oxford Functional Neurosurgery, Department of Neurosurgery, Radcliffe Infirmary, Woodstock Road, Oxford OX2 6HE, UK*
[e]*The Movement Disorders and Neurostimulation Group, Department of Neuroscience, Charing Cross Hospital & Division of Neurosciences and Mental Health, Imperial College London, Fulham Palace Road, London W6 8RF, UK*

Received 31 January 2006; accepted 29 June 2006

Abstract

Functional correlation between oscillatory neural and muscular signals during tremor can be revealed by coherence estimation. The coherence value in a defined frequency range reveals the interaction strength between the two signals. However, coherence estimation does not provide directional information, preventing the further dissection of the relationship between the two interacting signals. We have therefore investigated causal correlations between the subthalamic nucleus (STN) and muscle in Parkinsonian tremor using adaptive Granger autoregressive (AR) modeling. During resting tremor we analyzed the inter-dependence of local field potentials (LFPs) recorded from the STN and surface electromyograms (EMGs) recorded from the contralateral forearm muscles using an adaptive Granger causality based on AR modeling with a running window to reveal the time-dependent causal influences between the LFP and EMG signals in comparison with coherence estimation. Our results showed that during persistent tremor, there was a directional causality predominantly from EMGs to LFPs corresponding to the significant coherence between LFPs and EMGs at the tremor frequency; and over episodes of transient resting tremor,

*Corresponding author. Tel.: +44 2088467631; fax: +44 2083830663.
E-mail addresses: shou.wang@physiol.ox.ac.uk (S. Wang), ychen@bme.ufl.edu (Y. Chen), mding@bme.ufl.edu (M. Ding), jianfeng.feng@warwick.ac.uk (J. Feng), john.stein@physiol.ox.ac.uk (J.F. Stein), tipu.aziz@physiol.ox.ac.uk (T.Z. Aziz), x.liu@ic.ac.uk (X. Liu).

doi:10.1016/j.jfranklin.2006.06.003

the inter-dependence between EMGs and LFPs was bi-directional and alternatively varied with time. Further time–frequency analysis showed a significant suppression in the beta band (10–30 Hz) power of the STN LFPs preceded the onset of resting tremor which was presented as the increases in the power at the tremor frequency (3.0–4.5 Hz) in both STN LFPs and surface EMGs. We conclude that the functional correlation between the STN and muscle is dynamic, bi-directional, and dependent on the tremor status. The Granger causality and time–frequency analysis are effective to characterize the dynamic correlation of the transient or intermittent events between simultaneously recorded neural and muscular signals at the same and across different frequencies.

Keywords: Causality; Coherence; Autoregressive model; Time–frequency; Local field potential; Electromyogram

1. Introduction

The electrical signals produced by the nervous system offer a unique opportunity to explore the brain processes in real time. Electroencephalogram (EEG) recorded from the scalp has been extensively used in clinical diagnostic and basic neuroscience research, which has proved essential in understanding of the function of the cerebral cortex in healthy subjects and patients since the pivotal pioneering work of Hans Berger [1]. Recently, the therapy of deep brain stimulation (DBS) makes it possible to carry out recordings from deep structures of human brain [2]. The local field potentials (LFPs) recorded directly via the implanted DBS electrode reflect the coherent neuronal population activity [3]. Such recordings are valuable for understanding the pathophysiology of disorders and provide insights into the basic mechanisms of brain functions such as movement control, perception, memory formation, and even conscious awareness. Furthermore, these signals provide the information on the dynamic functional coupling of the different levels of the human nervous system.

Analysis of functional coupling between muscular activity and simultaneously recorded oscillatory neural activity at different levels of the motor system has led not only to a better understanding of the pathophysiological mechanisms of movement disorders [4] but also to better localization of targets for DBS [5]. One widely used method of estimating the functional coupling between two oscillatory signals is the magnitude-squared coherence (MSC). The MSC is a normalized cross-spectral density function, and measures the strength of association and relative linearity between two stationary processes on a scale from zero to one [6–8]. The coherence value indicates the strength of the coupling in the frequency domain between two signals. The conditional coupling among multiple signals may be further measured by partial coherence [9,10]. However, these techniques based on correlation or coherence are not sufficient to describe the interdependence among signals. Similar significant coherence estimation may appear in both systems with and without feedback. Thus, it does not help to elucidate any causal relationships within the system. Therefore, to fully understand information processing at different levels of the motor system, directional interaction analysis to reveal causal influence between signals is essential to uncover the basic mechanisms underlying the motor system.

The causal relations were described initially as probabilistic concept, which is that one variable may be caused by the other if it can be better predicted by incorporating knowledge of the second one. Granger formulated the concept in terms of predictability

based on the linear regression models of stochastic processes [11]. The causality was expressed as one time series is caused by the other one if its prediction error at the present time can be reduced by including the past of the second one in the model. Geweke's work based on multivariate autoregressive (AR) process expended Granger causality into the spectral representation [12] and conditional causality measurement [13]. In a recent study, Granger analysis was performed for oscillatory field potential activity in the beta (14–30 Hz) frequency range among sensorimotor cortical recording sites during a GO/NO–GO visual pattern discrimination task in monkeys [14]. Some other equivalent methods, for instance directed transfer function [15], partial directed coherence [16], were also used to describe the information flow in the brain structure [17,18], and recently the causal inference based on a graphical model was further developed [19] and applied to evaluate the connectivity in neural systems [20].

Stationarity of the neural and muscular signals usually relates to the state or specific physiological/pathological condition over which the signal is recorded. Most of the neural signals exhibit non-stationary characteristics to some extent. In particular, the tremor activity can be transient and intermittent. To investigate the dynamic changing of the causal relationship between the neural and muscular signals, the time-variant causality analysis is needed. Moreover the time–frequency analysis has the advantage of obtaining the dynamic information in both time and frequency domains and investigating the interaction across frequency. In the present study, we performed windowed Granger causality analysis to quantify the time-dependent coupling between two simultaneously recorded neural and muscular signals. LFPs were recorded via the DBS electrode implanted in the subthalamic nucleus (STN). The electromyograms (EMGs) recorded from the skin surface over the selected muscles can be considered a stochastic (zero–mean) process resulting from the electrical activity of activated muscle fibers. In contrast to oscillatory neural signals, the physiological output from the central motor system is usually encoded in the 'envelope' of the compound EMG signal rather than in the individual action potentials of muscle fibers. We pre-processed the EMG signals, validated our AR models, and investigated influence of noise and the time-dependent causality with running window. We then used Granger causality analysis to reveal any causal correlation between STN LFPs and the EMGs of forearm muscles in Parkinsonian patients with sustained or intermittent resting tremor. The dynamic changes in the components at the tremor frequency and the beta frequency band of the STN LFPs over a transient tremor episode was further investigated using short-time Fourier transform in both time and frequency domains.

2. Methods

2.1. Description of coherence and Granger causality

AR representations of wide-sense stationary time series $x_1(t)$ and $x_2(t)$ are

$$x_1(t) = \sum_{k=1}^{\infty} a_1(k)x_1(t-k) + u_1(t), \tag{1}$$

$$x_2(t) = \sum_{k=1}^{\infty} a_2(k)x_2(t-k) + u_2(t), \tag{2}$$

where the parameters $a_1(k)$ and $a_2(k)$ are the model coefficients, $u_1(t)$ and $u_2(t)$ are the prediction error when $x_1(t)$ and $x_2(t)$ are predicted from its own past, respectively. The variance of $u_1(t)$ and $u_2(t)$ are Σ_1 and Σ_2.

The linear dependence between these two signals can be expressed as a bivariate AR model

$$x_1(t) = \sum_{k=1}^{\infty} a_{11}(k)x_1(t-k) + \sum_{k=1}^{\infty} a_{12}(k)x_2(t-k) + v_1(t), \tag{3}$$

$$x_2(t) = \sum_{k=1}^{\infty} a_{21}(k)x_1(t-k) + \sum_{k=1}^{\infty} a_{22}(k)x_2(t-k) + v_2(t), \tag{4}$$

where the parameters $a_{ij}(k)$ are the model coefficients, $v_1(t)$ is the prediction error when $x_I(t)$ is predicted from its own past and past of $x_2(t)$, and similarly for $v_2(t)$. The above equations can be expressed in the matrix form as $X(t) = [x_1(t), x_2(t)]^{\mathrm{T}}$, $V(t) = [v_1(t), v_2(t)]^{\mathrm{T}}$ and

$$\mathbf{A}(k) = -\begin{bmatrix} a_{11}(k) & a_{12}(k) \\ a_{21}(k) & a_{22}(k) \end{bmatrix}$$

(superscript T stands for transpose), then

$$X(t) = -\sum_{k=1}^{\infty} \mathrm{A}(k)X(t-k) + V(t). \tag{5}$$

Let $\mathbf{A}(0) = \mathrm{I}$, the identity matrix, Eq. (5) can be re-written as

$$\sum_{k=0}^{\infty} \mathbf{A}(k)X(t-k) = V(t). \tag{6}$$

The spectral relationship of Eq. (6) can be written as $\mathbf{A}(f)\mathbf{X}(f) = \mathbf{V}(f)$, in which $\mathbf{X}(f) = \mathbf{A}^{-1}(f)\mathbf{V}(f) = \mathbf{H}(f)\mathbf{V}(f)$ and

$$\mathbf{A}(f) = \sum_{k=0}^{\infty} \mathbf{A}(k)\mathrm{e}^{-\mathrm{i}k2\pi f}. \tag{7}$$

The power spectral matrix of the signals is then given by

$$\mathbf{S}(f) = \mathbf{X}(f)\mathbf{X}^*(f) = \mathbf{H}(f)\mathbf{V}(f)\mathbf{V}^*(f)\mathbf{H}^*(f) = \mathbf{H}(f)\sum \mathbf{H}^*(f),$$

where * stands for conjugate transpose

$$\Sigma = \begin{bmatrix} \Sigma_{11} & \Sigma_{12} \\ \Sigma_{21} & \Sigma_{22} \end{bmatrix},$$

is the co-variance matrix of $v_1(t)$ and $v_2(t)$ and, and

$$\mathbf{S}(f) = \begin{bmatrix} S_{11}(f) & S_{12}(f) \\ S_{21}(f) & S_{22}(f) \end{bmatrix},$$

is the spectral matrix of $x_1(t)$ and $x_2(t)$ and, where $S_{11}(f)$ and $S_{22}(f)$ are the auto-spectra of $x_1(t)$ and $x_2(t)$ and $S_{12}(f)$ and $S_{21}(f)$ are their cross-spectra.

The MSC is defined as the normalized cross-spectral density by the autospectral densities [7,21]:

$$\gamma_{xy}^2(f) = \frac{|S_{12}(f)|^2}{S_{11}(f)S_{22}(f)}.$$

The measure of Granger causality from $x_2(t)$ and $x_1(t)$ is defined as $F_{x_2\to x_1} = \ln(\Sigma_1/\Sigma_{11})$. $F_{x_2\to x_1}$ is nonnegative. If $\Sigma_1 = \Sigma_{11}$, $F_{x_2\to x_1} = 0$ which indicates $x_2(t)$ does not cause $x_1(t)$ [12]. The measure of $F_{x_2\to x_1}$ is invariant when $x_2(t)$ and $x_1(t)$ are rescaled or pre-multiplied by different invertible lag operators. Symmetrically, the measure of causality from $x_1(t)$ to $x_2(t)$ is defined as $F_{x_1\to x_2} = \ln(\Sigma_2/\Sigma_{22})$.

The causality $F_{x_2\to x_1}$ measures the reduction in the total variance of predictive errors of $x_1(t)$ when past $x_2(t)$ is added for prediction and used as their causality measure $F_{x_2\to x_1}$. The percentage reduction of the variance $R^2 = 1 - e^{-F_{x_2\to x_1}}$ suggests the degree of $x_1(t)$ relating to the history of $x_2(t)$.

$F_{x_2\to x_1}$ can be decomposed in frequency domain [12] as

$$F_{x_1\to x_2}(f) = \ln\frac{|S_{22}(f)|}{|S_{22}(f) - H_{21}(f)(\Sigma_{11} - \Sigma_{12}^2/\Sigma_{22})H_{21}^*(f)|}$$

and

$$F_{x_2\to x_1}(f) = \ln\frac{|S_{11}(f)|}{|S_{11}(f) - H_{12}(f)(\Sigma_{22} - \Sigma_{12}^2/\Sigma_{11})H_{12}^*(f)|}.$$

The normalized causality measures are given as

$$R_{x_2\to x_1}^2(f) = 1 - e^{-F_{x_2\to x_1}(f)}, \tag{8}$$

$$R_{x_1\to x_2}^2(f) = 1 - e^{-F_{x_1\to x_2}(f)}, \tag{9}$$

in the scale of 0 to 1.

2.2. Selection and validation of AR models

The optimal model order is determined according to the criteria, which are usually based on the statistics constructed from prediction errors. Akaike's information criterion (AIC) $\mathrm{AIC}(i) = N\log(\det(\hat{\Sigma}_i) + 2L^2 i$ is the most commonly used one, where $\hat{\Sigma}_i$ is the estimate of the prediction error covariance matrix assuming an ith-order model, N is the number of data points and L is the number of variables. AIC should be computed only for a maximum value of i of $3\sqrt{N}/L$ in order to produce reliable results. The optimal model order corresponds to the minimum of $\mathrm{AIC}(i)$.

The model can be validated by assessing the quality of the model fitness of the prediction ratio [22], which measures how much the model can explain the variance of the signal, and the percentage of the variance contributed from the model in the total variance. This provides objective criteria on whether the model is capable of characterize the system dynamics. For perfect fitness, the prediction error is zero. If the model is correct and the true parameter values are estimated properly, the prediction error would be white noise. If the autocorrelation function shows pronounced patterns, such as the ripples or slow decline at low lags, it suggests model inadequacy.

We determined the optimal model order for recordings from each patient according to AIC and validated the model with the prediction ratio and autocorrelation of the prediction error.

2.3. Short-window coherence and causality analysis

To obtain the time-dependent evolution of coherence and causality estimations in frequency of the signals considered to be locally stationary [23], estimations were performed using a running time-window. The window has a relative short duration with overlapping, so the estimation reflects the properties of the time-localized signals. By successively sliding the window over time and adaptively estimating the model parameters in each window, one can obtain a coherence or causality distribution of the signals in time–frequency domain.

In the present study, we selected a 3s window as it is longer than three times of the model order, and gives adequate time and frequency resolutions for observing the resting tremor of predominant 4.8 Hz within a band of 0–30 Hz with events of its onset and offset occurring over a few seconds.

2.4. Short-time fourier transform

STFT is Fourier spectra analysis with time-windows of limited length and maps time-domain signals onto an integrated time–frequency spectrogram. The frequency characteristics are localized by the pre-defined time-window. The STFT of signal $x(t)$ is defined as

$$\mathrm{STFT}(t,f) = \int x(\tau)\gamma^*(\tau - t)\mathrm{e}^{-\mathrm{j}2\pi f\tau}\,\mathrm{d}\tau. \tag{10}$$

For a digital signal $x(k)$, $k = 0 \ldots L-1$, STFT is extended to

$$\mathrm{STFT}(k,n) = \sum_{i=0}^{L-1} x(i)\gamma^*(i-k)W_L^{-ni} = \mathrm{STFT}(t,f)\big|_{t=k\Delta t, f=n/(L\Delta t)}, \tag{11}$$

where Δt is the sampling interval, and $\gamma(\cdot)$ is a symmetric window of usually a short time duration. STFT localizes the signal using the time-window running through the signal to obtain a windowed spectrum of signal $x(t)$ at time t, to multiply the signal by the window function $\gamma(\cdot)$ centered at time t, and then to compute the Fourier transform of the product. The window function has a relative short duration, so the Fourier transform of the product reflects the frequency properties of the time-localized signal. By successively sliding the window over time, one can obtain a distribution of the signal in time–frequency domain. The presentation of the spectrogram can be smoothed further when the overlapping of windows is applied, as each time step for plotting the spectrogram becomes less than the window width. Furthermore, window overlapping increases data points for more accurate subsequent regression analysis.

The results short-time Fourier transform is usually presented as a spectrogram.

$$\mathrm{SP}(k,n) = \left|\sum_{i=0}^{L-1} x(i)\gamma^*(i-k)W_L^{-ni}\right|^2. \tag{12}$$

It gives the energy distribution of the signal along both time and frequency axis.

In the present study, we selected a Hanning window of 3 s in length for the reason that we intended to observe the intermittent resting tremor of predominant 4.8 Hz within a band of 0–30 Hz, the events of its onset and offset occurred over a few seconds, and the signals were sampled at a rate of 4000 Hz. This setting gives a time resolution of 3 s and a frequency resolution of 0.3 Hz approximately, which are adequate for our purpose.

2.5. Signal recording and pre-processing

The study was approved by the local research ethics committee, and informed consent was obtained from each of five patients with resting tremor due to PD who underwent chronic stimulation in both STNs at the Radcliffe Infirmary, Oxford. Detailed surgical procedures and target localization have been described previously [24]. Patients underwent bilateral implantation of quadripolar DBS electrodes (3389, Medtronic, Mineapolis, USA) in STN. The implanted DBS electrode had 4×1.5 mm contacts, each separated by 0.5 mm. The bipolar recordings were made 4–6 days post-operatively from adjacent pairs of the externalized electrode. Localization of the electrode was confirmed by post-operative magnetic resonance imaging. EMGs were recorded using surface electrodes placed in a tripolar configuration over the tremulous forearm extensor and flexors. Signals were amplified using isolated CED 1902 amplifiers ($\times$ 10,000 for LFPs and $\times$ 1000 for EMGs), filtered at 0.5–500 Hz and digitized using CED 1401 mark II at 4000 Hz using Spike2 (Cambridge Electronic Design, Cambridge, UK).

The EMGs were high-pass filtered above 15 Hz using wavelet transforms to remove the motion artifacts. Then the EMGs were rectified in order to extract the EMG envelope signal. Both rectified EMGs and LFPs were low-pass filtered (corner frequency: 30 Hz). Then both signals were down-sampled to 100 Hz and detrended for further coherence, causality and time–frequency analysis. All signals were processed using MATLAB (Version 6.5, MathWorks Inc., Natick, MA, USA).

3. Results

3.1. Pre-processing

The surface EMGs were a compound signal of multi-unit activity and had a broad frequency distribution. The tremor-related activity, presented as synchronized rhythmic bursts at 5 Hz (Fig. 1(A)) independent of the individual muscle fiber action potentials. The tremor bursts were isolated firstly by performing full-wave rectification (Fig. 1(B)) and further by extracting the envelope following low-pass filtering the rectified EMGs and down-sampling at 100 Hz (Fig. 1(C)). Similar filtering and down sampling were performed on the LFP signals.

3.2. Selection and validation of AR model

The optimal model order of the bivariate AR model of each pair of LFP and EMG signals was determined from the AIC curve (Fig. 2). The AIC curve dropped as the model order increased and it became flat when the order was larger than 17 in this particular case.

The selected model for each individual signal pair was then validated by the prediction error. The prediction ratio of LFPs was 0.72, 0.74, 0.74 and 0.75 and that of EMGs was

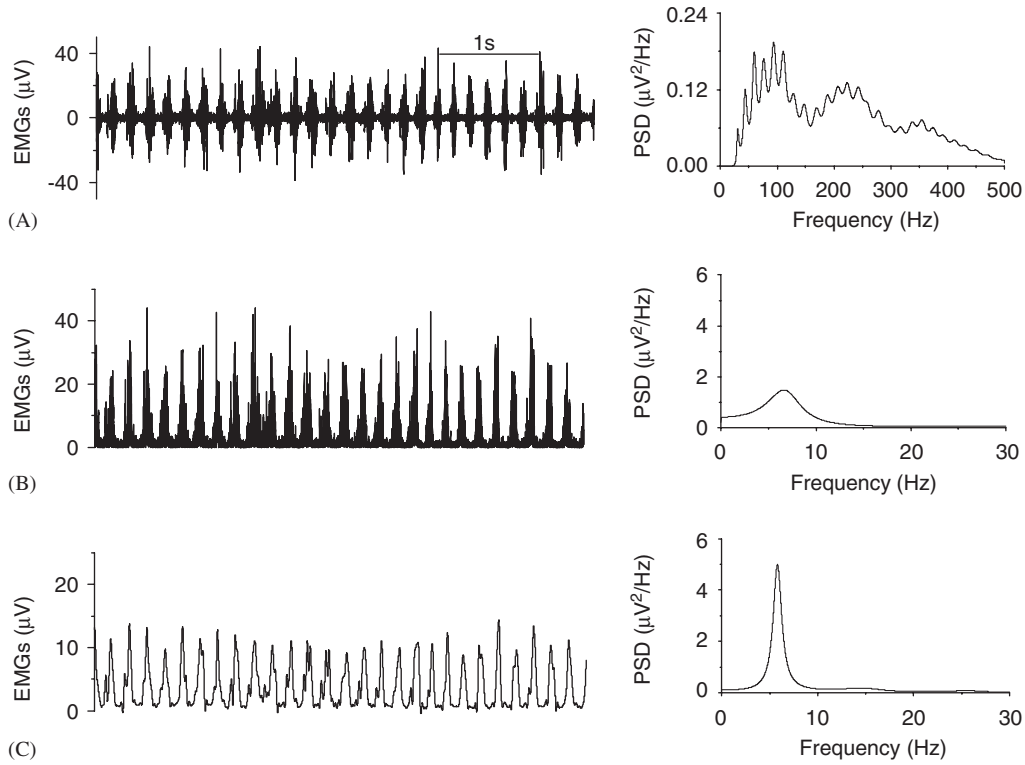

Fig. 1. Extracting the envelope of the tremor bursts in the surface EMG signal: (A) EMG signal of multi-unit activity with a broad frequency distribution; (B) full-wave rectification to enhance the tremor rhythmic bursts; and (C) extracting the envelope of the tremor bursts by low-pass filtering and down sampling.

0.91, 0.92, 0.93 and 0.94 when the model order was 10, 15, 20 and 25. Although the efficiency of the model was not significantly improved by increasing the order, the structure of the prediction error changed. When the model order was 10 and 15, the auto-correlation of the prediction error exhibited gradually decreasing pattern with ripples along the time delay axis (Fig. 3(A) and (B)); whereas when the order was 20 and 25, there was only one sharp peak at zero time delay (Fig. 3(C) and (D)). In this particular case, an order of 20 was selected.

3.3. *Influence of noise on coherence and causality analyses*

The influence of noise on coherence and causality was assessed by adding white noise to the EMG signal. A pair of LFP and EMG signals with 0%, 20%, 40%, 60%, 80% and 100% white noise in amplitude was analyzed for coherence and causality and compared. With increases in noise level, the coherence estimates at the tremor frequency of 5.2 Hz decreased from 0.96 at 0% noise to 0.87 at 100% noise (Fig. 4). Interestingly, the influence of noise on causality estimates was related to the directional correlation between the LFPs and EMGs: the causality value at the tremor frequency of 5.2 Hz increased as the noise

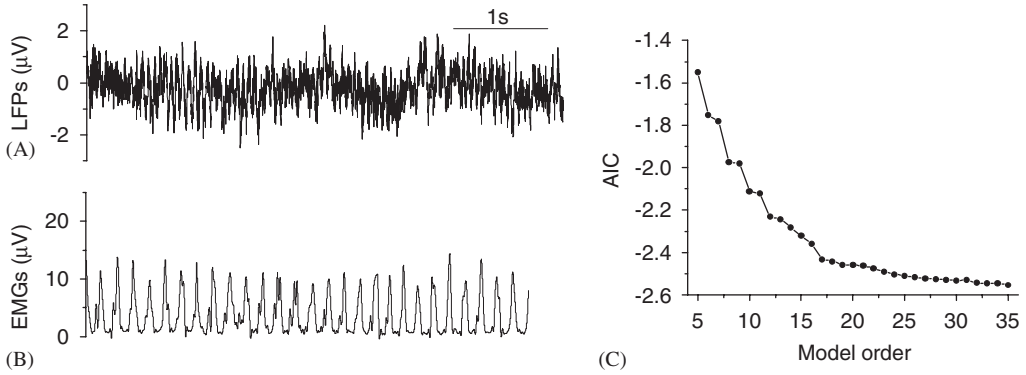

Fig. 2. The AIC curve of the bivariate AR model (C) between the processed LFPs (A) and EMGs (B).

level increased when the causality value was insignificant from LFPs to EMGs; whereas the effect of noise on causality estimation was reversed when the causality value is significant from EMGs to LFPs (Fig. 4).

3.4. Coherence and causality estimation between STN LFPs and EMGs in PD patients with persistent resting tremor

The coherence and causality were computed between STN LFPs and EMGs from four PD patients during persistent resting tremor (Fig. 5). The coherence estimate at the tremor frequency was 0.83 ± 0.13 (mean $\pm$ SD) averaged across 4 patients. The mean causality was 0.17 ± 0.04 from LFPs to EMGs; whereas 0.66 ± 0.14 ($p < 0.01$, paired t-test) from EMGs to LFPs at the tremor frequency.

3.5. Time-dependent coherence and causality estimation between STN LFPs and EMGs over intermittent tremor

The windowed coherence and causality analyses were performed to reveal the dynamic changes in the correlation between the STN LFPs and EMGs over a period of intermittent resting tremor in one of the four patients. As the tremor being unstable over time (Fig. 6(A)), the coherence (Fig. 6(B) and (E)) and causality (Fig. 6(C), (D) and (F)) estimates varied accordingly at the tremor (4.5 Hz) and the double-tremor (9.0 Hz) frequencies. In this particular case, intermittent tremor appeared at most of the time, and there was predominant causality from EMGs to LFPs; whereas the causality changed to the opposite direction when tremor activity reduced or even ceased (Fig. 6(F)).

3.6. Dynamic changes in the tremor and beta band activity of the STN

The dynamic changes of the simultaneously recorded STN LFPs and EMGs over a period of intermittent resting tremor were investigated using STFT. Fig. 7 shows the raw signals and the spectrogram of simultaneously recorded STN LFPs (Fig. 7(A)) and surface EMGs of the contralateral forearm extensor (Fig. 7(B)) over the onset of resting tremor. In relation to the onset of resting tremor, the spectrogram of the STN LFPs shows a

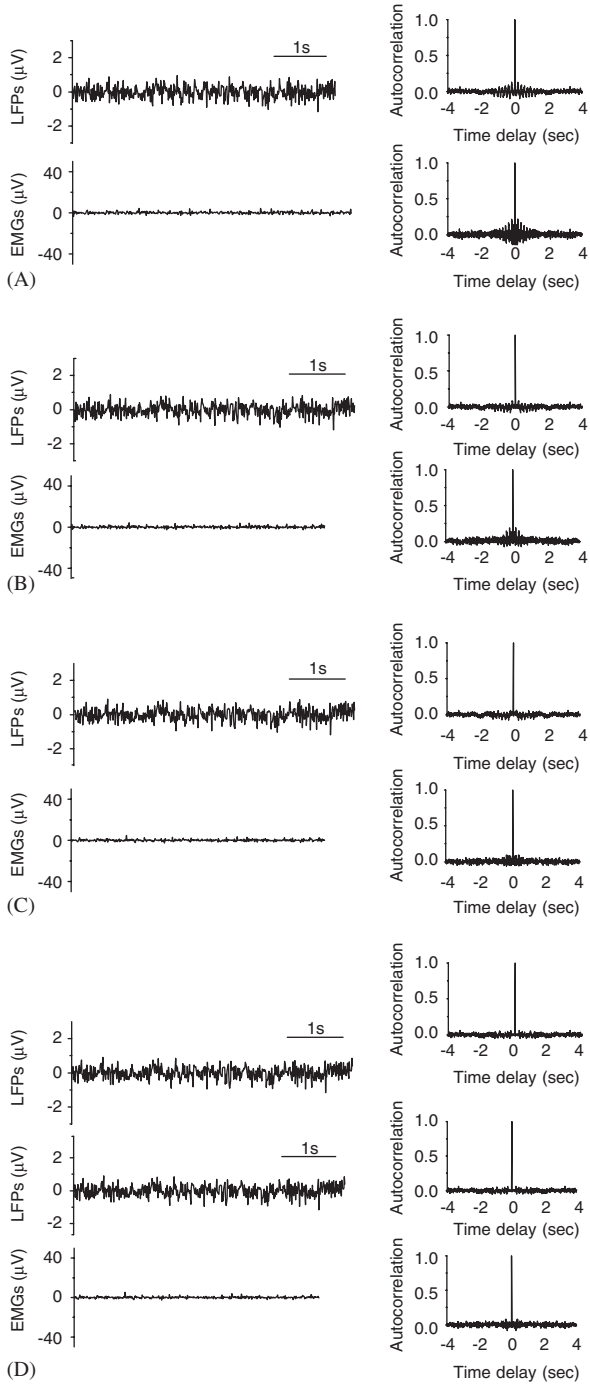

Fig. 3. The prediction error and its auto-correlation of LFPs and EMG envelope signals from the model with orders of 10 (A), 15 (B), 20 (C) and 25 (D).

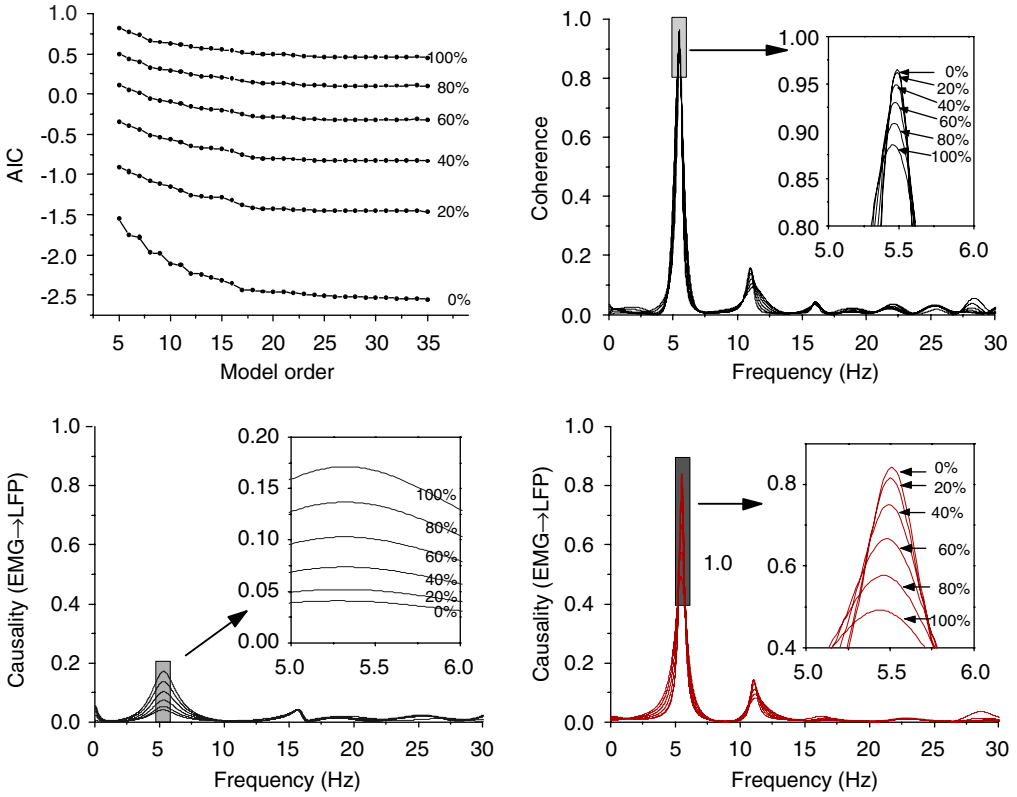

Fig. 4. The influence of white noise on coherence and causality estimation between STN LFPs and EMGs.

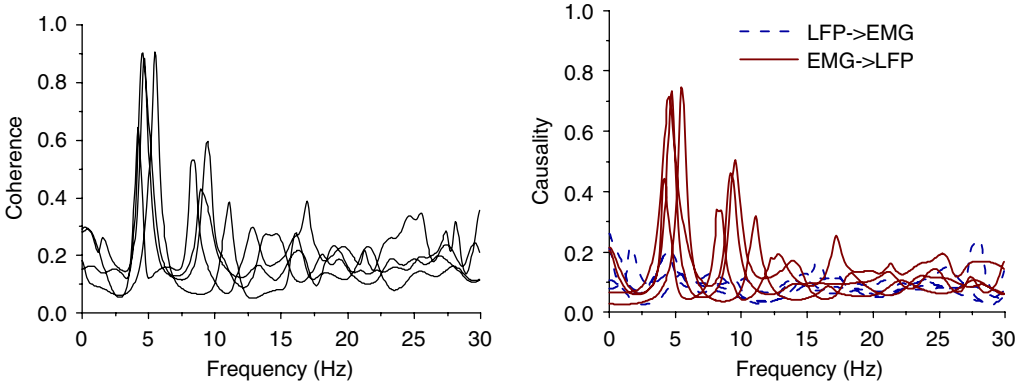

Fig. 5. Coherence and causality analysis of four PD patients with persistent resting tremor.

significant suppression in the range of 10–30 Hz (the beta band) appears around the 12th to 13th second and an increase in power at the tremor frequency of 4.6 Hz appearing at the 18th second. Meanwhile, rhythmic tremor bursts appears in the EMGs at the 18th second in association with two strong narrow bands at the tremor and double-tremor frequencies

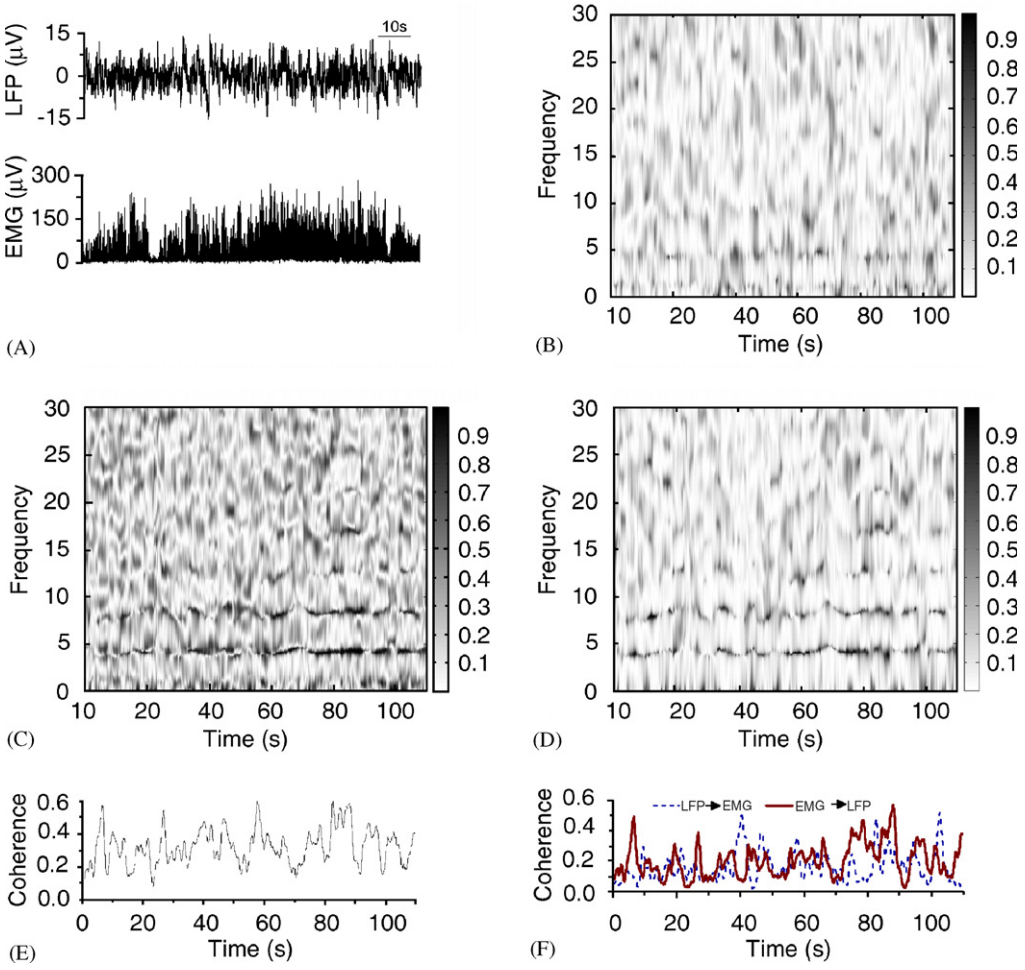

Fig. 6. STN LFPs and EMGs of intermittent tremor (A), time-dependant coherence (C) and causality spectrograms (B and D) and their mean values around tremor frequency (E and F).

and a general increase in activity across the entire displayed frequency range in the EMG spectrogram. The power values over the beta band (10–30 Hz) of LFP spectrogram and tremor band of both LFP and EMG spectrograms were averaged and compared (Fig. 7(C)). The power of the STN LFPs in the beta band decreased significantly about 5–6 s preceding the power increases at the tremor frequency in both STN LFPs and EMGs over the onset of resting tremor.

4. Discussion

We used Granger causality to analyze the directional influences between the LFPs of the STN and EMGs of the contralateral arm muscles in patients with Parkinsonian resting tremor to compare with standard coherence estimation. Windowed coherence and causality analyses and time–frequency analysis could be used to reveal time-dependent

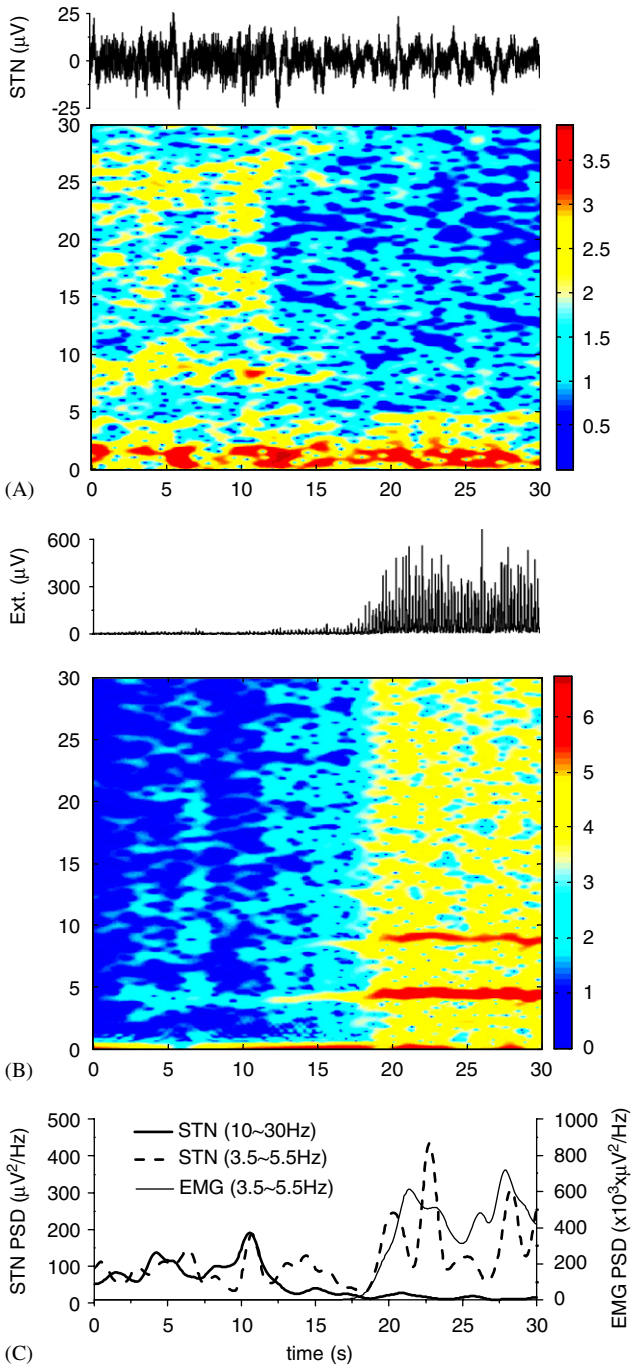

Fig. 7. STN LFPs (A) and EMGs (B) over the onset of resting tremor and their STFT spectrograms. The averaged beta band power in the LFPs (10–30 Hz, thick solid line) showed a significant suppression preceding the onset of resting tremor reflected by the increases in the power at the tremor frequency band (3.0–4.5 Hz) in both LFPs (dashed line) and EMGs (thin solid line) (C).

changes related to the intermittent tremor at and across tremor and beta band frequencies. The pre-processing of EMG signals, selection and validation of AR models and influence of signal noise were investigated.

Whereas LFPs and EEGs are compound neural signals, surface EMGs result from spatial and temporal interference between muscle motor unit action potentials. Action potentials in the surface EMGs exhibit a broad frequency distribution up to 500 Hz. Tremor causes synchronized bursts of action potentials in the surface EMGs, but the features of the tremor burst are independent of those of the action potentials. Actually they are encoded in the envelope of the EMG bursts. Therefore, pre-processing the surface EMGs to extract the tremor burst envelope is essential for further correlation analysis. Full-wave rectification is an effective way to do this and enhance the tremor component in the EMGs. Further low-pass filtering may reduce high-frequency noise which is above the frequency range of interest (<30 Hz). Finally, down-sampling the EMGs completes the extraction of the tremor envelope signal.

The proper selection and validation of an AR model is necessary for further analysis but is not straightforward in practice. A linear model is usually a simple starting point. In this study, the validation of a model is based on the statistics derived from the prediction error, for instance, the prediction ratio and autocorrelation of prediction error. On the one hand, these criteria are objective for determining the efficiency, fitness and propriety of a model structure. On the other hand, there may be more factors contributing to the variability of a system giving a model of a low prediction ratio and unclear autocorrelation. In this case, a non-linear or time-dependent model is more suitable to characterize the system. The prediction ratio was in the range from 70% to 97% when an AR model was identified at the optimal order with proper autocorrelation structure of prediction error. Furthermore, we selected and validated the AR model adaptively for each pair of LFP-EMG signals.

Both coherence and causality analysis may be influenced by waveform distortion. Neither LFPs nor EMG envelopes are perfect sine waves, which leads to production of harmonics. In addition, signal noise is a significant influential factor. The noise decreases the efficiency of the coherence estimation so that the estimates are smaller than their true values. For causality estimation, the noise reduced the proportion of tremor-related component in EMG signal and increased the amplitude of the prediction error in the bivariate AR model. As a result, the noise in EMG signal decreases the causality measure in one direction and increases in the other direction. In an extreme situation, the high level noise or the non-tremor-related activity in the LFPs or EMGs may obscure the true causality. In this study, the significant causality was found from muscle to STN during stable Parkinsonian resting tremor.

Dynamic correlation across time and frequency between the intermittent tremor-related activity in the STN and muscles were quantified using windowed coherence and causality analyses. For this purpose, the AR model provides adequate frequency resolution even when a short data segment is used. The length of running window determines the time resolution. The length of time window is determined as it is large enough to cover the entire cycle of the dominant component in the signals. In practice, the reliable identification of a model with order 20 needs one second long LFPs and EMGs recording at least. Stationarity of the signals is another issue when the windowed causality analysis is considered. It usually relates to the state or specific physiological or pathological condition over which the signals are recorded.

Previous work has found that beta suppression precedes timed voluntary hand movements following a visual cue [25] and the degree of synchronization of STN activity in the beta band may be related to motor programming and movement initiation [26]. Our present results of the interaction between the beta band and tremor frequency activity in STN LFPs revealed using short-time Fourier transform showed that there was a significant correlation over time between the powers of these two components in different frequency bands. The suppression in beta band activity in the STN preceded the onset of activity at the tremor frequency in the STN and muscle. We speculate that the beta activity may present a resting state of the STN, which may be suppressed over the tremor occurrence.

In conclusion, the Granger causality and time–frequency analysis are effective approaches to characterize the dynamic causal correlation of the transient or intermittent events between simultaneously recorded neural and muscular signals at the same and cross different frequencies. The directional inter-dependence of the tremor-related STN LFP-EMG coupling varied with time and highly related to the tremor states.

Acknowledgments

We would like to express our gratitude to patients and to the Norman Collisson Foundation, the Medical Research Council, UK and NIMH, USA, for their support.

References

[1] H. Berger, Uber das elektrenkephalogramm des menschen (On the EEG in humans), Arch. Psychiatr. Nervenkr. 87 (1929) 527–570.
[2] A.K. Engel, C.K. Moll, I. Fried, G.A. Ojemann, Invasive recordings from the human brain: clinical insights and beyond, Nat. Rev. Neurosci. 6 (2005) 35–47.
[3] X. Liu, What can be learned from recording local field potentials from the brain via implanted electrodes used to treat patients with movement disorders? Current Mory activity in the Parkinsonian subthalamic nucleus investigated using the macredical literature, Neurology 19 (2003) 1–6.
[4] X. Liu, H.L. Ford-Dunn, G.N. Hayward, D. Nandi, R.C. Miall, T.Z. Aziz, J.F. Stein, The oscillato-electrodes for deep brain stimulation, Clin. Neurophysiol. 113 (2002) 1667–1672.
[5] C.C. Chen, A. Pogosyan, L.U. Zrinzo, S. Tisch, P. Limousin, K. Ashkan, T. Yousry, M.I. Hariz, P. Brown, Intra-operative recordings of local field potentials can help localize the subthalamic nucleus in Parkinson's disease surgery, Exp. Neurol. 198 (2006) 214–221.
[6] S.Y. Wang, X. Liu, J. Yianni, C. Miall, T. Aziz, F. Stein, Optimising coherence estimation to assess the functional correlation of tremor-related activity between the subthalamic nucleus and the forearm muscles, J. Neurosci. Methods 136 (2004) 197–205.
[7] G.C. Carter, Coherence and time delay estimation, Proc. IEEE 75 (1987) 236–255.
[8] D. Brillinger, Time Series: Data Analysis and Theory, McGraw-Hill, New York, 1981.
[9] J.R. Rosenberg, D.M. Halliday, P. Breeze, B.A. Conway, Identification of patterns of neuronal connectivity-partial spectra, partial coherence, and neuronal interactions, J. Neurosci. Methods 83 (1998) 57–72.
[10] Z. Albo, G.V. Di Prisco, Y. Chen, G. Rangarajan, W. Truccolo, J. Feng, R.P. Vertes, M. Ding, Is partial coherence a viable technique for identifying generators of neural oscillations?, Biol. Cybern. 90 (2004) 318–326.
[11] C.-W.J. Granger, Investigating causal relations by econometric models and cross-spectral methods, Econometrica 37 (1969) 424–438.
[12] J. Geweke, Measurement of linear dependence and feedback between multiple time series, J. Am. Stat. Assoc. 77 (1982) 304–313.
[13] J. Geweke, Measurement of conditional linear dependence and feedback between time series, J. Am. Stat. Assoc. 79 (1984) 907–915.

[14] A. Brovelli, M. Ding, A. Ledberg, Y. Chen, R. Nakamura, S.L. Bressler, Beta oscillations in a large-scale sensorimotor cortical network: directional influences revealed by Granger causality, Proc. Natl. Acad. Sci. USA 101 (2004) 9849–9854.
[15] M.J. Kaminski, K.J. Blinowska, A new method of the description of the information flow in the brain structures, Biol. Cybern. 65 (1991) 203–210.
[16] L.A. Baccala, K. Sameshima, Partial directed coherence: a new concept in neural structure determination, Biol. Cybern. 84 (2001) 463–474.
[17] M. Winterhalder, B. Schelter, W. Hesse, K. Schwab, L. Leistritz, D. Klan, R. Bauer, J. Timmer, H. Witte, Comparison of linear signal processing techniques to infer directed interactions in multivariate neural systems, Signal Process. 85 (2005) 2137–2160.
[18] M. Kaminski, H. Liang, Causal influence: advances in neurosignal analysis, Crit. Rev. Biomed. Eng 33 (2005) 347–430.
[19] J. Pearl, Statistics and causal inference: a review, Test 12 (2003) 281–345.
[20] M. Eichler, A graphical approach for evaluating effective connectivity in neural systems, Philos. Trans. R. Soc. B 360 (2005) 953–967.
[21] D.M. Halliday, J.R. Rosenberg, A.M. Amjad, P. Breeze, B.A. Conway, S.F. Farmer, A framework for the analysis of mixed time series/point process data-theory and application to the study of physiological tremor, single motor unit discharges and electromyograms, Prog. Biophys. Mol. Biol. 64 (1995) 237–278.
[22] L. Ljung, System Identification: Theory for the User, second ed, Prentice-Hall, Upper Saddle River, NJ, 1999.
[23] M. Ding, S.L. Bressler, W. Yang, H. Liang, Short-window spectral analysis of cortical event-related potentials by adaptive multivariate autoregressive modeling: data preprocessing, model validation, and variability assessment, Biol. Cybern. 83 (2000) 35–45.
[24] X. Liu, J. Rowe, D. Nandi, G. Hayward, S. Parkin, J. Stein, T. Aziz, Localisation of the subthalamic nucleus using radionics image fusion(TM) and stereoplan(TM) combined with field potential recording: a technical note, Stereotact. Funct. Neurosurg. 76 (2001) 63–73.
[25] D. Williams, A. Kuhn, A. Kupsch, M. Tijssen, G. van Bruggen, H. Speelman, G. Hotton, K. Yarrow, P. Brown, Behavioural cues are associated with modulations of synchronous oscillations in the human subthalamic nucleus, Brain 126 (2003) 1975–1985.
[26] A.A. Kuhn, D. Williams, A. Kupsch, P. Limousin, M. Hariz, G.H. Schneider, K. Yarrow, P. Brown, Event-related beta desynchronization in human subthalamic nucleus correlates with motor performance, Brain 127 (2004) 735–746.